J. Fluid Mech. (1976), *vol.* 75, *part* 1, *pp.* 1–15
Printed in Great Britain

Taylor-vortex instability and annulus-length effects

By J. A. COLE

Mechanical Engineering Department,
University of Western Australia, Nedlands

(Received 26 August 1975)

Critical speeds for the onset of Taylor vortices and for the later development of wavy vortices have been determined from torque measurements and visual observations on concentric cylinders of radius ratios $R_1/R_2 = 0{\cdot}894$–$0{\cdot}954$ for a range of values of the clearance c and length L: $c/R_1 = 0{\cdot}0478$–$0{\cdot}119$ and $L/c = 1$–107. Effectively zero variation of the Taylor critical speed with annulus length was observed. The speed at the onset of wavy vortices was found to increase considerably as the annulus length was reduced and theoretical predictions are realistic only for L/c values exceeding say 40. The results were similar for all four clearance ratios examined. Preliminary measurements on eccentrically positioned cylinders with $c/R_1 = 0{\cdot}119$ showed corresponding effects.

1. Introduction

The classical theoretical analysis by G. I. Taylor of the instability of circumferential laminar flow between rotating cylinders dealt with coaxial cylinders assumed to have infinite length L and infinitesimally small annular clearance c. Subsequent analyses of the onset of axisymmetric Taylor vortices have been broader, dealing with finite clearances (for concentric cylinders) or with eccentricity (for small clearances), but the assumption of infinite length has so far remained. Similarly, the analysis by Davey, DiPrima & Stuart (1968) of the stability of Taylor-vortex flow was also restricted to coaxial cylinders of infinite length and small clearance, but the recent analysis by Eagles (1971) of the onset of periodic or wavy vortices has avoided the small-clearance assumption. Experimental studies of these flow instabilities are customarily made using long cylinders, probably with the aim of reproducing as far as is practicable the infinite-length conditions of the theory, although short cylinders are more likely to be encountered in engineering applications.

Taylor vortices do occur in very short annuli and visual observations described later show that a single counter-rotating vortex pair can form in an open-ended annulus less than two radial clearances long and that the wavy mode can be observed in an annulus containing only five vortex cells. The present paper gives experimental results on the effect of annulus length on the critical speeds at which Taylor vortices and subsequently wavy vortices form, dealing primarily with concentric cylinders and considering length/clearance ratios L/c from 1 to 107. The general conclusion is that only the critical speed for the onset of wavy

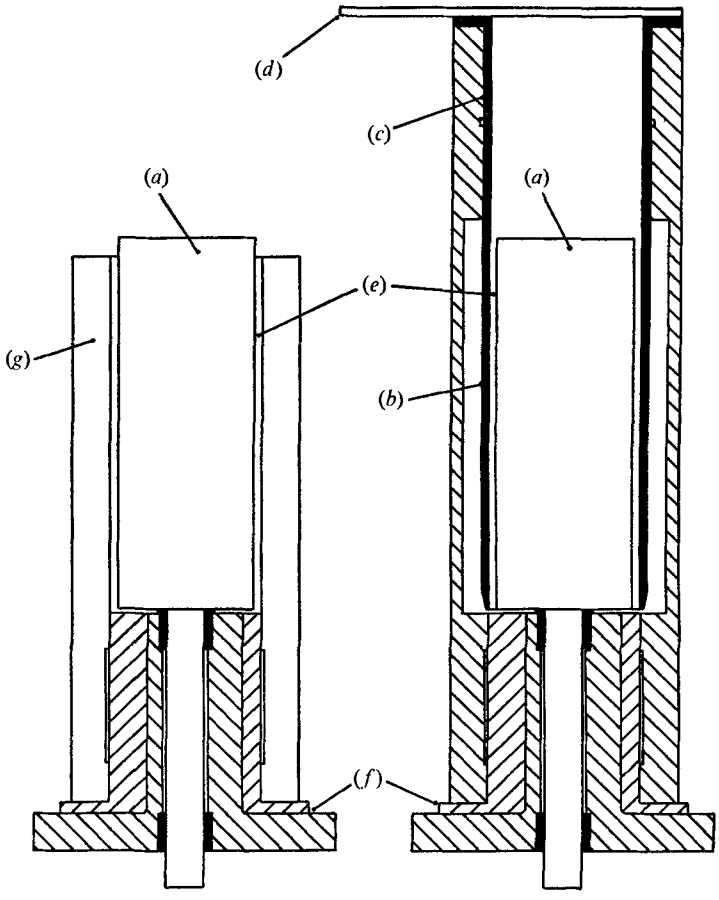

FIGURE 1. Test rig (diagrammatic). (*a*) Rotor (diameter 91·42 or 95·45 mm). (*b*) Floating stator (bore 100·01 mm). (*c*) Air bearing. (*d*) Torque arm. (*e*) Test annulus. (*f*) Eccentricity adjustment. (*g*) Perspex stator (bore 102·30 mm).

vortices is significantly affected by reduction of annulus length, particularly for L/c values below say 40. Snyder (1969*b*) has stated that end effects are important when L/c falls below 10, but he was concerned with flow-history phenomena and the non-uniqueness of Taylor-vortex cell patterns, with reference to experiments at speeds usually well above the critical values for Taylor vortices (Snyder 1969*a*) and for wavy vortices (Coles 1965; Snyder 1969*b*).

2. Apparatus and experimental method

Two methods of detecting the flow instabilities are used here, namely torque measurement and flow visualization, but unfortunately the equipment does not permit their use simultaneously. The test rig, illustrated in figure 1, was developed for an earlier investigation (Cole 1969) of the effect of eccentricity on Taylor-vortex onset and employs a vertical steel rotor supported at its lower end in two plain bearings which are in turn mounted in a double eccentric sleeve so as to

Figure number	3(*a*)	5(*a*)	3(*b*)	5(*b*)
Clearance ratio, c/R_1	0·0478	0·0718	0·0940	0·1190
Radius ratio, R_1/R_2	0·954	0·933	0·914	0·894
Viscosity, ν (cS)	6·10	2·97	15·6	19·3
Observation method	Torque	Visual	Torque	Visual
Maximum length, L/c	107	67	61	45
Taylor vortices				
†Calculated $\sqrt{T}$	41·8	42·2	42·5	42·8
Observed $\sqrt{T}$ at max L/c	41·7	42·3	43·0	42·7
Observed $\sqrt{T}$ at $L/c = 20$	42·2	41·8	43·0	42·7
Wavy vortices				
‡Calculated $\sqrt{T}$ $m = 1, 2$	44·1	44·4	44·7	45·0
‡Calculated $\sqrt{T}$ $m = 4$	44·5	44·8	45·1	45·4
Observed $\sqrt{T}$ at max L/c	45·1	45·4	47·4	47·8
Observed $\sqrt{T}$ at $L/c = 20$	52·2	50·5	52·0	51·7

† Values interpolated from numerical results by Walowit, Tsao & DiPrima (1964).

‡ Values calculated from $\sqrt{T} = 43{\cdot}5\,(1 + 0{\cdot}291c/R_1)$ for $m = 1, 2$ and $\sqrt{T} = 43{\cdot}9 \times (1 + 0{\cdot}291c/R_1)$ for $m = 4$, expressions derived from the finite-clearance analysis by Eagles (1971) giving numerical results for $c/R_1 = 0{\cdot}0515$ and from the small-clearance analysis by Weinstein (1975) showing that the effect of clearance ratio is represented by the term $1 + 0{\cdot}291c/R_1$.

(Observed values are taken from the mean curves in the figures)

TABLE 1. Dimensionless critical speeds $\sqrt{T} = \dfrac{2\pi N R_1 c}{\nu}\left(\dfrac{2c}{R_1 + R_2}\right)^{\frac{1}{2}}$.

permit offsetting of the rotor relative to the surrounding stator. The steel stator consists of two parts, the outer having an externally pressurized air bearing at its upper end to provide a frictionless support for the inner part, allowing measurement of the torque reaction on the latter. The force transducer is an unbonded strain gauge, maximum load either 0·02 or 0·1 N, coupled to a digital voltmeter and an X, Y recorder. The rotor is driven through a worm gear box by a servo-controlled variable-speed d.c. motor, with speed measurement by a perforated disk and photocell system coupled to a counter and also to a frequency meter and the X, Y recorder. Rotor speeds, here 0·02–3 rev/s, can be set and held constant for several hours if necessary to an accuracy of better than 0·1 % and can be measured to within better than 0·01 % of the maximum. Automatic point plotting or continuous recording of torque–speed graphs can be performed using a synchronous motor to drive either stepwise or continuously the multi-turn potentiometer controlling the motor speed. The test rig is operated in a temperature-controlled room, and the fluid temperature is measured with a thermistor acting as a resistance thermometer, the same thermistor being used during standard U-tube viscometry on the test fluids, silicone oils. Viscosities are listed in table 1. The annulus length is varied by altering the depth of silicone oil in the rig and is measured using an external sight tube and a cathetometer. The end conditions are asymmetric, the annulus being bounded by a stationary solid surface at the lower end and by a free liquid surface at the upper end.

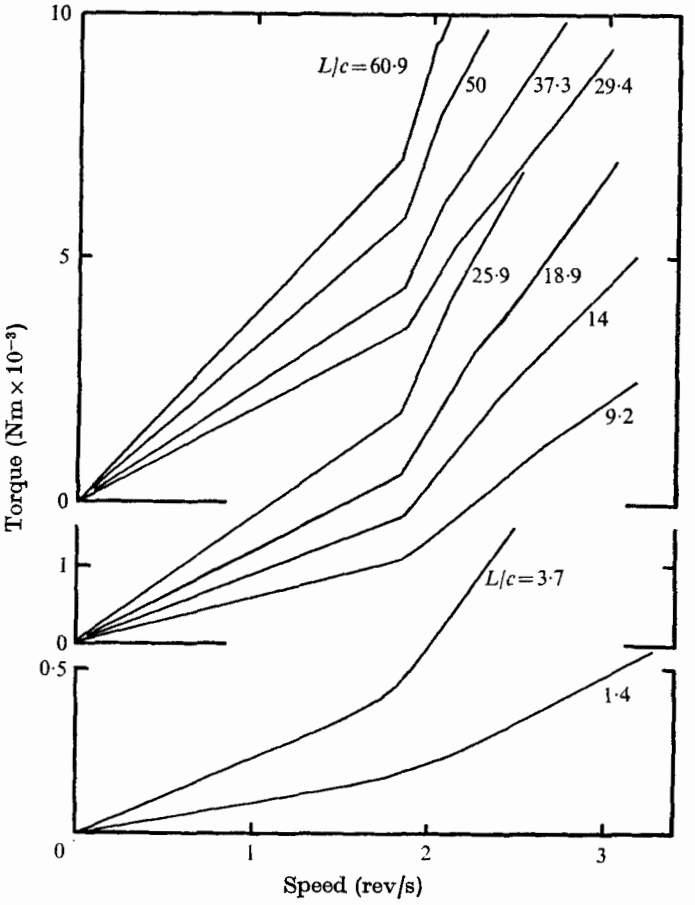

FIGURE 2. Recorded torque–speed curves: $c/R_1 = 0{\cdot}0940$.

For flow-visualization experiments, the complete stator unit is replaced by a thick Perspex outer cylinder and flow patterns are shown up by adding a small quantity of aluminium flakes (typical maximum dimension 0·01 mm) to the silicone oil. A viscometric check showed that the viscosity was not measurably affected by this addition.

3. Torque measurements

The first experiments on length effects involved torque measurements, prompted by the observation of poorly defined critical conditions while extending the earlier investigation (Cole 1969) of eccentricity effects to large clearances, which in turn involved the use of low length/clearance ratios.

Figure 2 shows observed torque–speed relationships for a range of fluid depths using cylinders of clearance ratio $c/R_1 = 0{\cdot}0940$. The scale of the figure makes it impracticable to show the very large number of individual points recorded when using the automatic point-plotting technique with small speed increments and

only the mean lines are shown. The critical speed for the onset of Taylor vortices is indicated by a pronounced increase in the slope of the torque–speed relationship: for all depths, the gradient in the Taylor-vortex regime is approximately 3·2 times the laminar value here.

However, the change in slope is not sharp at smaller fluid depths, the rounding becoming perceptible at $L/c = 8$–10, and the critical speed is then taken to occur at the intersection of the extrapolated linear portions of the plot. At $L/c = 1{\cdot}41$, the lowest depth shown in figure 2, comparable flow-visualization experiments show only a single vortex cell but the torque–speed graph still resembles those for the onset of Taylor vortices at greater annulus lengths although the slope change is very gradual; the intersection of the extrapolated linear portions of the graph occurs at a speed approximately 8% in excess of the expected Taylor critical speed. The rounding of the torque graph at low fluid depths could arise from the relatively greater contribution of parasitic viscous drag on the chamfered end of the floating outer cylinder and of autorotation drag of the externally pressurized air bearing but these effects are believed to be unimportant. Similar rounding has been encountered with this rig when using large fluid depths and very large clearances, so that only a few vortex cells were set up but torques were more easily measured, and it is believed that a rounded torque–speed relationship is characteristic of small cell numbers. In this connexion, attention is drawn to the theoretical result of Benjamin (1975) that cylinders of finite length are subject to subcritical instability.

As the rotor speed is further increased above the Taylor critical value, a second gradient change is seen, now downward and less pronounced, and this corresponds to the onset of wavy vortices. At the maximum fluid depth in figure 2, the gradient in the Taylor-vortex regime is about 50% higher than that in the wavy-vortex regime and the critical condition is again sharply indicated, but as the fluid depth is reduced the downturn becomes less marked and the ratio of the gradients tends to unity as L/c falls below 10, so that clear-cut indications of the wavy critical condition can no longer be obtained from torque measurements.

Figures 3(*a*) and (*b*) give the critical speeds† determined from torque measurements using two clearances, $c/R_1 = 0{\cdot}0478$ and $0{\cdot}0940$, and show that the Taylor critical speed is virtually unaffected by annulus length, taking into account the uncertainty in deciding the critical condition for very short annuli. The wavy critical speed on the other hand is markedly affected by annulus length, rising appreciably as L/c is reduced below 40. The experimental observations are compared with theoretical values of the critical speeds in table 1 and agreement is good in the case of the Taylor critical speeds. Theoretical predictions of the wavy critical speed are available only for $R_1/R_2 = 0{\cdot}951$ ($c/R_1 = 0{\cdot}0515$; see Davey *et al.* 1968; Eagles 1971) but a recent analysis by Weinstein (1975) gives an indication of the effect of the clearance ratio and this has been used in table 1 to extrapolate from Eagles' results. The entries in table 1 for the larger of the two clearances used in the torque experiments show a

† Expressed as N rev/s and also non-dimensionally as $\sqrt{T}$, defined in table 1.

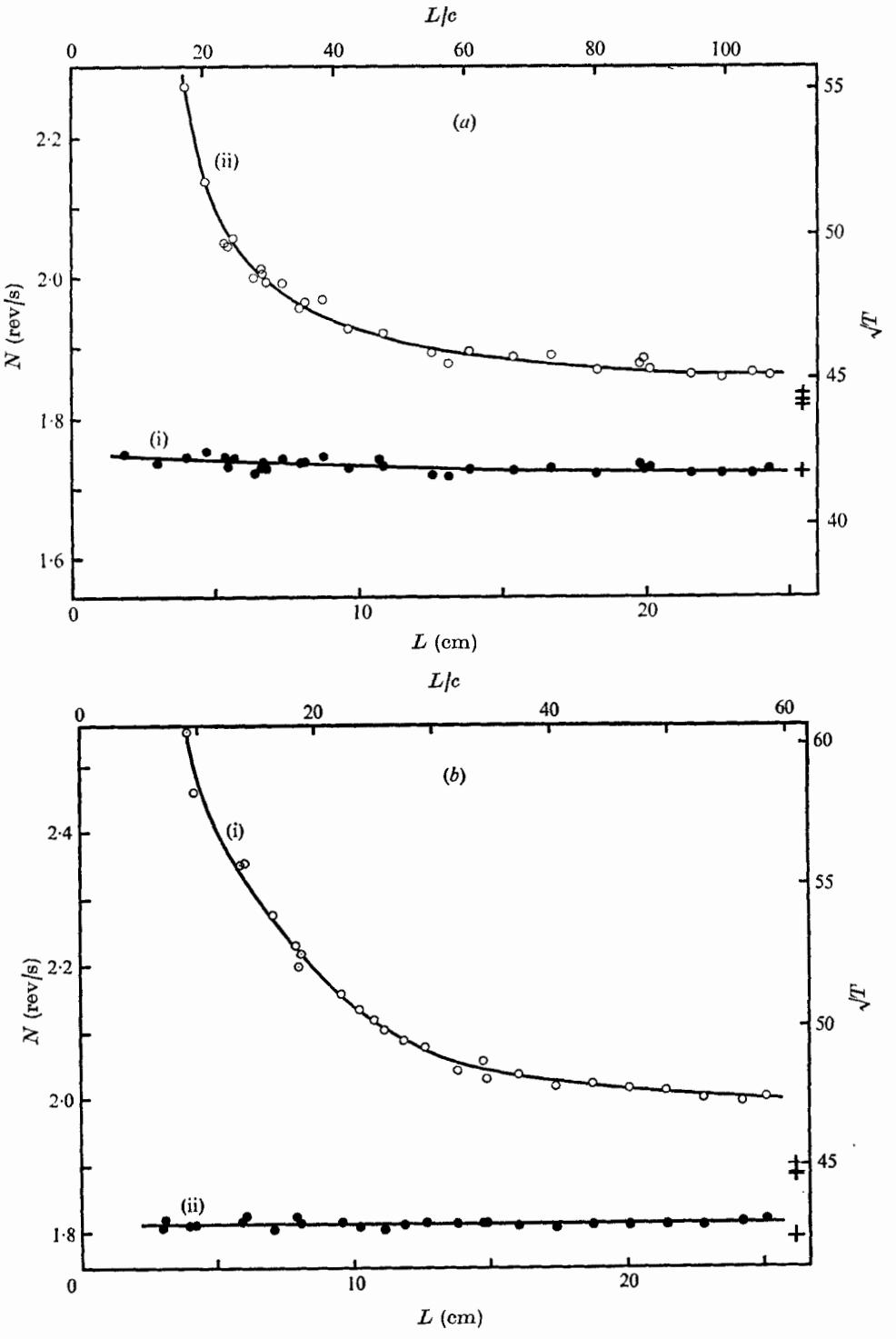

FIGURE 3. Critical speeds for onset of (i) Taylor and (ii) wavy vortices determined from torque measurements: (*a*) $c/R_1 = 0{\cdot}0478$, (*b*) $c/R_1 = 0{\cdot}0940$. +, theoretical predictions (see table 1).

measured wavy critical speed 5–6 % in excess of the calculated values even at the maximum L/c value of 61. This may reflect a combination of residual annulus-length effects, experimental error and theory extrapolation error. For the smaller clearance, the discrepancies are smaller, 1–2 %, probably because the length effect is smaller with the higher L/c value of 107 and because less extrapolation was needed for the calculated wavy critical speed. The experimental determinations of both critical speeds were usually repeatable to within about $\pm 0{\cdot}5$ %, better than this at larger fluid depths and rather worse at smaller depths. Hence the maximum experimental errors in the tabulated dimensionless critical speeds are assessed at approximately 1 % after taking into account also the contributions of less than 0·2 % from errors in measuring the smallest cylinder clearance and 0·3 % from errors in measuring temperature and viscosity.

4. Visual observations

As the rotor speed is gradually increased from zero, observation of aluminium particles mixed with the silicone oil shows that shadowy vortex pairs appear at the ends of the annulus at speeds as low as 70–80 % of the expected Taylor critical speed and that the vortex pattern develops by spreading axially inwards as the speed is raised further. Measurements of cell sizes in the cell formation stage, using the cathetometer with some difficulty, show that initially the height of a single vortex cell (other than an end cell) equals the radial clearance, as expected. Completion of the pattern with an integral number of vortex cells, of equal size apart from the anomalously large cell at each end of the annulus, may involve a cell-size adjustment process. In the case of rapid acceleration of the rotor from rest to a speed above critical, this cell-size adjustment process has been observed (Cole 1974*a*) to hinge on a minimum survival size for the vortex pair formed last, but here, with gradual acceleration to the critical speed, the process is obscure. It is tempting nevertheless to suggest that the number of cells finally occurring in a given annulus will still depend on whether the last-formed vortex cell or pair of cells can survive as the pattern adjusts for cell-size equality. Figure 4 shows the number of cells finally present at the critical speed for various annulus lengths with a clearance ratio $c/R_1 = 0{\cdot}119$. The annulus lengths at which the number of cells changes are sharply defined and are linearly related as indicated: extrapolation suggests that odd numbers of cells will not occur at values of L/c exceeding 46, just beyond the rig capability. With larger clearances, odd numbers of cells were found to occur only at much shorter annulus lengths.

Detection of the actual critical speed for Taylor vortices by visual observation is not always clear-cut, particularly for small annulus lengths and for lengths at which the number of cells changes. Otherwise, the speed at which all divisions between individual cells just become visible has been found to agree well with the calculated critical speed.

By contrast, the detection of the onset of wavy vortices by the aluminium-particle visualization technique is highly satisfactory, provided that direct observation and not still photography is used. The presence of the wave profile

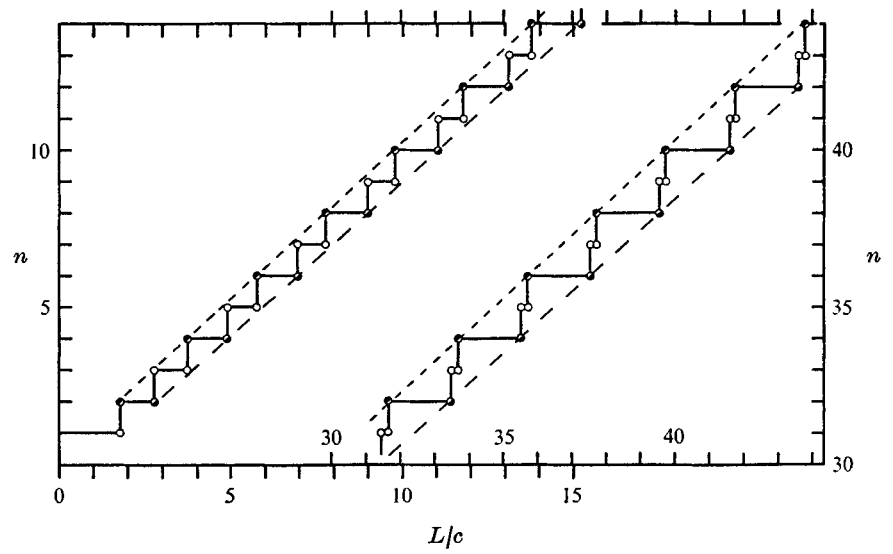

FIGURE 4. Variation of number of vortex cells n with annulus length L/c for gradual acceleration to Taylor critical speed: $c/R_1 = 0{\cdot}1190$ (points for $16 \leqslant L/c \leqslant 30$ not shown). Upper dashed line (best fit for 22 successive ◐ values of n): $n = 1{\cdot}00L/c + 0{\cdot}25$. Lower dashed line (best fit for 21 successive ◑ values of n): $n = 0{\cdot}98L/c - 0{\cdot}82$.

is easily perceived visually because of the sensitivity of the eye to the small transverse motion as the wave travels round the cylinder even though the amplitude of the wave may be so small as not to be measurable on a photograph. As with the appearance of Taylor vortices, there seems to be no hysteresis effect with speed increases and decreases, but whereas Taylor-vortex completeness seemed to be more easily detected with the speed rising, wave motion seemed to be more easily judged by its cessation with the speed falling.

Two cylinder clearance ratios $c/R_1 = 0{\cdot}0718$ and $0{\cdot}119$ were examined visually in order to overlap the two clearances of the torque experiments, giving an overall clearance range of 2·5 : 1, and the results are shown in figures 5 (*a*) and (*b*). These confirm the torque observations in showing that the Taylor critical speed is little affected by annulus length while the wavy critical speed rises substantially at small annulus lengths. However, the Taylor vortices are shown to appear in complete form slightly earlier when the annulus length is small, roughly where the torque observations become dubious owing to rounding in the slope-change region. At the largest values of L/c, the visual observations are in good agreement with calculated values of Taylor critical speeds, as shown in table 1, and in fairly good agreement with calculated wavy critical speeds, the discrepancies here being interpretable in the same way as those for the torque measurements.

The curves for the onset of wavy vortices cover a wider range of annulus lengths than was possible in the torque experiments, where the detection method became very insensitive with small lengths. Figure 6 combines the wavy critical observations for all four clearances, the critical speeds now being expressed as multiples of the appropriate theoretical values but with some uncertainty in

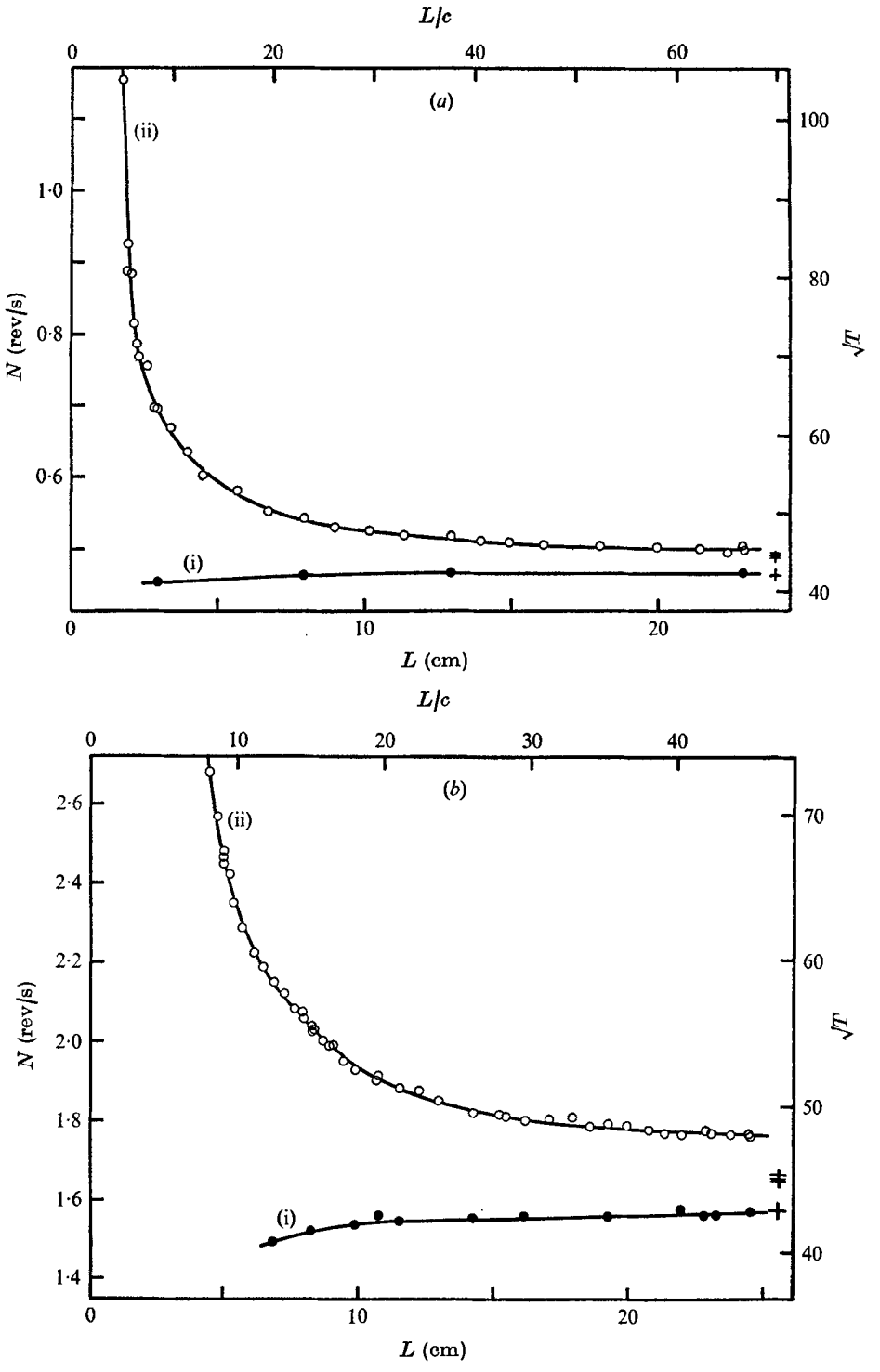

FIGURE 5. Critical speeds for onset of (i) Taylor and (ii) wavy vortices determined from visual observations: (*a*) $c/R_1 = 0{\cdot}0718$, (*b*) $c/R_1 = 0{\cdot}1190$. +, theoretical predictions (see table 1).

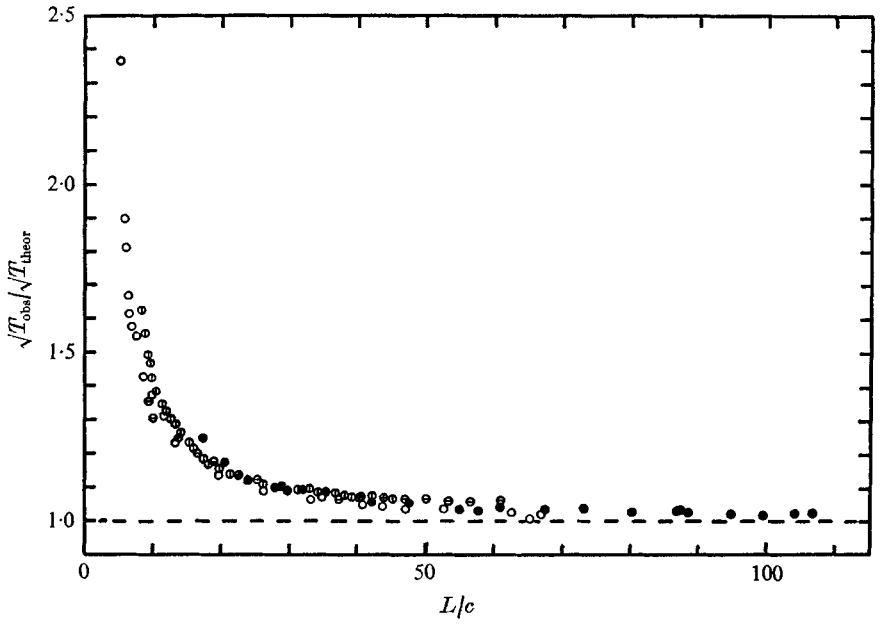

FIGURE 6. Variation with annulus length/clearance ratio of wavy-vortex critical speed expressed as a multiple of the theoretical value. ●, $c/R_1 = 0{\cdot}0478$ (torque); ⊖, $c/R_1 = 0{\cdot}0940$ (torque); ○, $c/R_1 = 0{\cdot}0718$ (visual); ⊙, $c/R_1 = 0{\cdot}1190$ (visual).

their comparison since three of the calculated values involve extrapolation. The four sets of points coalesce reasonably well, with a bandwidth of $\pm 2\,\%$ or less over a substantial part of the length range, and the greatest divergence occurs at short lengths, where the torque method is least accurate.

The conclusion to be drawn from figure 6 and table 1 is clear: the onset of wavy vortices occurs increasingly early as the annulus length is reduced for all four clearances tested and theoretical predictions of the critical speed based on current infinite-length theory are likely to be as much as 5 % too low at $L/c = 35$, 20 % too low at $L/c = 15$ and over 100 % too low at $L/c = 5$.

Theoretical predictions of the critical speed for the onset of wavy vortices show a small dependence on the wave mode m: the finite-clearance analysis by Eagles (1971) predicts an increase of 0·8 % for $m = 4$ and 0·1 % for $m = 2$ over the value for $m = 1$ for $R_1/R_2 = 0{\cdot}951$. During the present flow-visualization experiments the mode was clearly visible once the wave amplitude was well developed but was impossible to judge when the wave motion first appeared as then the amplitude was so small as to be undetectable even on a photograph. Under conditions of well-developed wave motion it was evident that low modes occurred at large annulus lengths and high modes at low annulus lengths, and it would be interesting to apply a photocell device to the detection of modes at wavy-vortex onset.

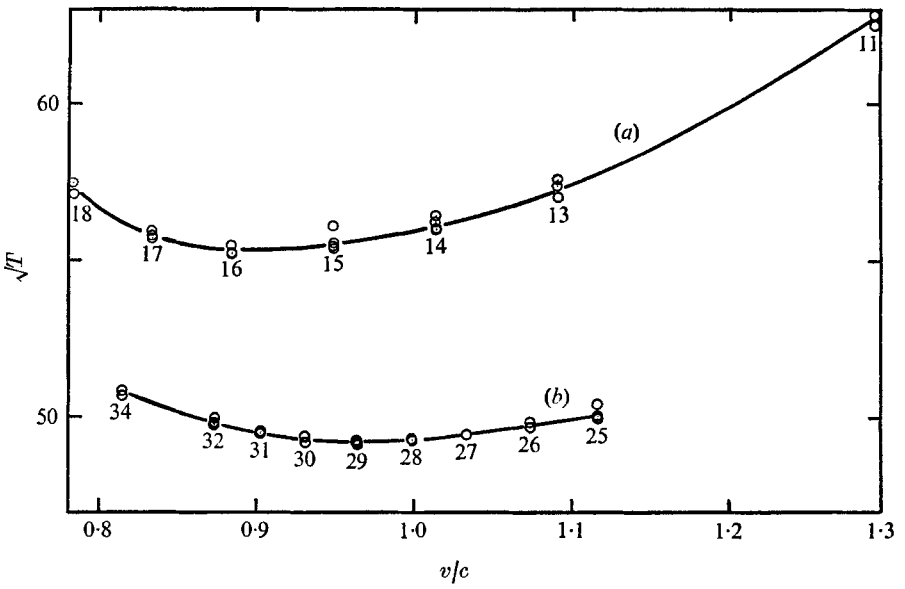

FIGURE 7. Variation of dimensionless wavy critical speed with mean vortex cell size for various annulus lengths: $c/R_1 = 0{\cdot}1190$. Numbers by points indicate total number of cells, but v is mean cell size excluding cell at each end of annulus. (*a*) $L/c = 14{\cdot}6$. (*b*) $L/c = 28{\cdot}4$.

Total number of cells	8		14		30		44	
Annulus length, L/c	7·7	9·0	13·8	15·1	29·7	31·4	43·7	45·7
†Measured cell size, v/c	0·92	1·06	0·95	1·05	0·98	1·03	0·98	1·03
‡Equivalent rise in Taylor critical speed	0·8%	0·4%	0·2%	0·3%	<0·1%	0·2%	<0·1%	0·2%

† Mean size excluding anomalously large cell at each end of annulus.
‡ Rise above minimum on theoretical stability curve.

TABLE 2. Measured vortex cell sizes for clearance ratio $c/R_1 = 0{\cdot}1190$

5. Vortex-size considerations

The predictions of critical speeds for the occurrence of Taylor vortices involve the assumption that the onset of the instability is represented by the minimum point on the theoretical stability curve relating the Taylor number and the disturbance wavenumber, and the appropriate wavenumber then turns out to correspond to a single vortex cell size v equal to the radial clearance c. In practice, depending on the flow history and on the annulus length, cell sizes are observed to vary considerably, by as much as $\pm 30\%$ from $v/c = 1$ (Cole 1974*b*). The results shown in figure 7, to be discussed later, are an illustration of this. With gradual acceleration to the critical speed for a fixed annulus length, the variation in cell size is smaller, and table 2 gives examples of measurements of extreme

cell sizes. The corresponding annulus lengths may be seen from figure 4 to be those at which changes in the number of cells occur. Also included in table 2 are the variations in the Taylor critical speed deduced from the theoretical stability curve for disturbance wavenumbers equivalent to the measured cell sizes. Except for the smallest annulus lengths, these variations do not exceed 0·3 % and would be very difficult to detect consistently using the present equipment even though they may account for some of the scatter in the points in figures 3 and 5. The variation of 0·8 % for $L/c = 7{\cdot}7$ would also be difficult to detect because, as noted earlier, the Taylor critical condition becomes somewhat vague at such small annulus lengths.

Dependence of the critical speed on cell size was detected also during the flow-visualization experiments on the onset of wavy vortices. The size of the Taylor vortices, once they were well established but not yet wavy, could be adjusted by the addition or subtraction of fluid to achieve a desired annulus length as described by the writer elsewhere (Cole 1974*b*), and wavy critical speeds could thus be determined for various cell sizes at that annulus length. Figure 7 shows observations of wavy critical speeds in terms of the number of cells, and hence the cell size, for two annulus lengths, $L/c = 14{\cdot}6$ and 28·4. Consistent operation was achieved over only a limited range of cell numbers and in particular 12 and 33 cells did not persist long enough for their critical speeds to be found. The maximum variation of the wavy critical speed is large, about 13 %, for the shorter annulus but it should be noted that the range of cell sizes in figure 7 is greater than would occur in the results shown in figures 3 and 5. There, only gradual acceleration at a series of unchanged annulus lengths was employed. Thus, from figure 4, 14 cells normally exist at $L/c = 14{\cdot}6$ and 28 cells at $L/c = 28{\cdot}4$, for which figure 7 suggests wavy critical speeds within a fraction of 1 % of the values for cells of size c.

6. The effect of eccentricity

The results of preliminary visual observations of the effect of eccentricity appear in figure 8 for one clearance ratio, $c/R_1 = 0{\cdot}119$. The critical speed for the onset of Taylor vortices rises as the offset e of the cylinder axes is increased and at an eccentricity ratio $e/c = 0{\cdot}25$ is 10 % higher than the concentric value, in good agreement with earlier results (Cole 1969, 1971), which have also shown that the effect of eccentricity is largely independent of the clearance ratio. Reducing the ratio L/c from the value corresponding to the results in figure 8 ($L/c = 45$) has little effect, in agreement with the preceding results on length effects. The dot–dash curve in figure 8 is the theoretical relationship derived by DiPrima & Stuart (1972, 1975) for the effect of eccentricity on the onset of Taylor vortices: at $e/c = 0{\cdot}25$, this predicts an increase in the critical speed of 8 % above the concentric value, close to that observed.

The critical speeds for the onset of wavy vortices in figure 8 also rise with an increase in eccentricity, with the separate curves for $L/c = 43{\cdot}7$ and 18·4 showing the dependence on annulus length. The dashed curve in figure 8 is a theoretical relationship derived by Weinstein (1975) for the effect of eccentricity on the

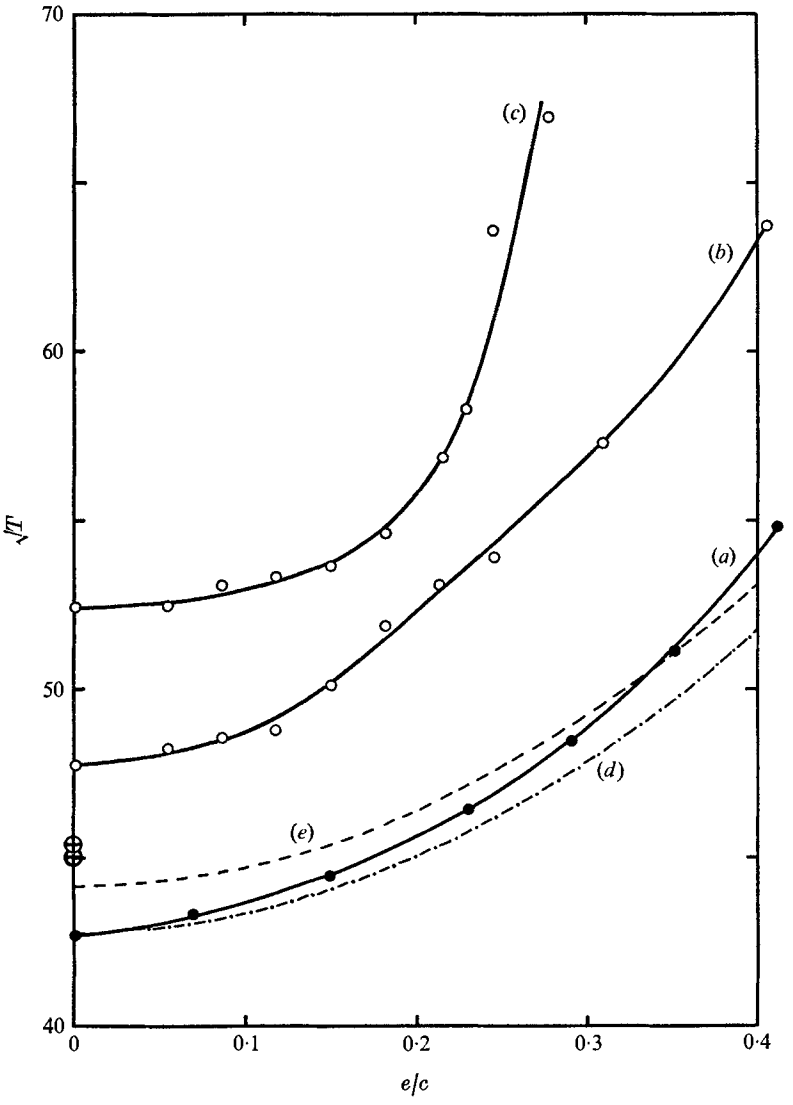

FIGURE 8. Variation of dimensionless critical speed $\sqrt{T}$ with eccentricity ratio e/c: $c/R_1 = 0{\cdot}1190$. (*a*) Taylor critical speed, $L/c = 45$. (*b*) Wavy critical speed, $L/c = 43{\cdot}7$. (*c*) Wavy critical speed, $L/c = 18{\cdot}4$. (*d*) $\sqrt{T} = 41{\cdot}2\,(1+0{\cdot}331c/R_1)\,[1+1{\cdot}312(e/c)^2]$ for Taylor critical speed (DiPrima & Stuart 1972, 1975). (*e*) $\sqrt{T} = 42{\cdot}7\,(1+0{\cdot}291c/R_1) \times [1+1{\cdot}273(e/c)^2]$ for wavy critical speed (Weinstein 1975). $\oplus$, calculated wavy critical speeds (see table 1).

onset of wavy vortices. This lies well below the experimental points, which, as noted earlier, may still be affected by length effects even for $L/c = 43{\cdot}7$: at $e/c = 0{\cdot}25$, the experimentally determined critical speeds are 14% above the concentric values, whereas Weinstein predicts an 8% increase. Visual observations of the wavy-vortex critical speed by Vohr (1968) for $c/R_1 = 0{\cdot}099$ and $L/c = 124$ show similar but smaller deviations from the theory: at $e/c = 0{\cdot}25$,

Vohr's experimental values are 12% above the concentric critical value while Weinstein again predicts an 8% increase. The onset of the wave instability becomes increasingly obscure as the eccentricity ratio rises above 0·3: the vortex cells tend to change size with the periodic onset of a helical swirling motion as the number of cells suddenly changes and it is then very difficult to decide whether the cells are in the true wavy mode.

7. Conclusion

These torque measurements and visual observations on rotating cylinders for four clearance ratios ranging from $c/R_1 = 0{\cdot}0478$ to 0·119 agree in indicating virtually no variation with annulus length of the critical speed for the onset of Taylor vortices, so that theoretical predictions are applicable for L/c values as low as say 8 and probably still lower. The critical speed for the onset of the wave instability of Taylor vortices, on the other hand, is markedly dependent on annulus length, and the indications are that current theoretical analyses are realistic only for $L/c > 40$ and that errors exceeding 15% can be expected at L/c values below 20. Eccentricity, which raises both critical speeds, produces similar length effects, but complicated flow patterns make visual observations difficult at eccentricity ratios above 0·3.

Grants for equipment from the Australian Research Grants Committee are acknowledged.

REFERENCES

BENJAMIN, T. B. 1975 The alliance of practical and analytical insights into the non-linear problems of fluid mechanics. *University of Essex Fluid Mech. Res. Inst. Rep.* no. 67.

COLE, J. A. 1969 Taylor vortices with eccentric rotating cylinders. *Nature*, **221**, 253–4.

COLE, J. A. 1971 Further experiments on Taylor vortices between eccentric rotating cylinders. *Proc. 4th Austral. Conf. on Hydraul. & Fluid Mech.*, pp. 27–34.

COLE, J. A. 1974*a* Taylor vortices with short rotating cylinders. *J. Fluids Engng*, **96**, 69–70.

COLE, J. A. 1974*b* Taylor vortex behaviour in annular clearances of limited length. *Proc. 5th Austral. Conf. on Hydraul. & Fluid Mech.*, pp. 514–21.

COLES, D. 1965 Transition in circular Couette flow. *J. Fluid Mech.* **21**, 385–425.

DAVEY, A., DIPRIMA, R. C. & STUART, J. T. 1968 On the instability of Taylor vortices. *J. Fluid Mech.* **31**, 17–52.

DIPRIMA, R. C. & STUART, J. T. 1972 Non-local effects in the stability of flow between eccentric rotating cylinders. *J. Fluid Mech.* **54**, 393–415.

DIPRIMA, R. C. & STUART, J. T. 1975 The nonlinear calculation of Taylor-vortex flow between eccentric rotating cylinders. *J. Fluid Mech.* **67**, 85–111.

EAGLES, P. M. 1971 On the stability of Taylor vortices by fifth-order amplitude expansions. *J. Fluid Mech.* **49**, 529–550.

SNYDER, H. A. 1969*a* Wave-number selection at finite amplitude in rotating Couette flow. *J. Fluid Mech.* **35**, 273–298.

SNYDER, H. A. 1969*b* Change in wave-form and mean flow associated with wavelength variations in rotating Couette flow. *J. Fluid Mech.* **35**, 337–352.

VOHR, J. H. 1968 An experimental study of Taylor vortices and turbulence in flow between eccentric rotating cylinders. *J. Lubrication Tech., Trans. A.S.M.E.* F **90**, 285–296.

WALOWIT, J., TSAO, S. & DIPRIMA, R. C. 1964 Stability of flow between arbitrarily spaced concentric cylindrical surfaces including the effect of a radial temperature gradient. *Trans. A.S.M.E.* E **86**, 585–593.

WEINSTEIN, M. 1975 Linear and non-linear instability between two eccentric cylinders. Ph.D. thesis, University of London.